UDC 621.396 DOI: 10.20535/2411-2976.22025.68-80

SIMULATION MODEL OF RADAR IMAGING TECHNIQUE WITH MODIFIED CW-LFM SAR

Volodymyr V. Pavlikov, Semen S. Zhyla, Danyil I. Kovalchuk, Denys V. Kolesnikov, Yaroslav D. Sydorov

National Aerospace University "Kharkiv Aviation Institute", Kharkiv, Ukraine

Background. Modern synthetic aperture radar (SAR) systems are crucial for Earth observation, especially in conditions where traditional optical systems fail, such as low visibility or adverse weather. Continuous wave linearly frequency modulated (CW-LFM) signals are promising for their energy efficiency and simplified hardware implementation, but they present significant signal processing challenges, including phase coherence preservation and spectral artifacts removal.

Objective. The study aims to develop and simulate a structural model of a compact SAR system based on CW-LFM signals, with a focus on improving image quality through advanced signal processing algorithms, specifically the use of decorrelation techniques for reference signals.

Methods. The study involves a mathematical formulation of radar imaging processes, development of a simulation model based on the proposed structural scheme, and implementation of signal processing operations such as quadrature detection, discrete Fourier transforms, and digital filtering. A new decorrelation method for reference signals is introduced and evaluated against classical approaches using various image quality metrics.

Results. Simulation results show that the proposed decorrelation technique improves image quality metrics, including SSIM, PSNR, and NCC. The method helps reduce speckle size and enhances image resolution. Artifacts caused by spectrum limitations were effectively suppressed using weighting functions. Quantitative evaluations using both real and artificially generated radar images confirmed the advantage of the proposed method over classical techniques.

Conclusions. The developed simulation model and signal processing improvements demonstrate the feasibility and effectiveness of using decorrelation-enhanced CW-LFM SAR systems for high-resolution radar imaging. The results can support further research and practical implementations in compact airborne and unmanned platforms for civil and defence applications.

Keywords: *synthetic aperture radar; CW-LFM signals; decorrelation; simulation model; image quality metrics.*

Introduction

In the modern system of the Earth remote sensing considerable attention is paid to the development of radars with a synthetic aperture (SAR), capable to form high-quality images regardless of weather conditions or illumination of the area. A particularly relevant task is the creation of small-sized SARs intended for use on unmanned platforms, which significantly expands the possibilities of applying technologies in the civil and defence spheres [1-3].

One of the promising approaches is the use of continuous linearly frequency modulated (CW-LFM) signals, which provide high energy efficiency, reduce the requirements for pulsed signal generation and simplify the hardware implementation of systems [4]. Despite the mentioned advantages, CW-LFM SAR is accompanied by several complex tasks: preserving phase coherence, minimising additive noise, synchronising digital paths and implementing optimal real-time signal processing.

A few studies [5-9] prove the effectiveness of statistical signal processing methods, in particular decorrelation and matched filtering methods, which allow improving the accuracy of reconstruction of spatial characteristics of the scene. However, there are still unresolved issues that limit the quality of operation of such systems, in particular: adaptive formation of reference signals taking into account the geometry of the aperture; elimination of spectral artifacts after decorrelation processing; improvement of resistance to low signal-to-noise ratio; effective digital implementation of convolution and filtering algorithms. To solve these problems, it is advisable to perform simulation modelling of various algorithms and probing signals.

In view of the above, the relevance of the study lies in the development and modelling of the structural scheme of a CW-LFM SAR, which ensures an optimal algorithm of radar imaging, stochastic structure of the complex scattering coefficient of the measurement object, measurement geometry, probability density of internal receiver noise and the parameters of probing signals.

Structural diagram of CW-LFM SAR

Based on an analysis of contemporary literature [1-5, 8, 9] and the results of the authors' development of optimal algorithms for processing spatio-temporal sig-

nals [6, 7], it follows that the general process of radar imaging can be described by two equations:

$$\left|\dot{Y}(x,y)\right|^2 = \left|\int_0^T u(t)\int_0^T W_u\left[t,t_1,\sigma^0(x,y)\right]\dot{s}_0(t_1,x,y)dt_1dt\right|^2, \quad (1)$$

$$\hat{\sigma}^0(x,y) = \frac{1}{2}\int_{-\infty}^{\infty}\int_{-\infty}^{\infty}\sigma^0(x_1,y_1)\left|\dot{\Psi}(x,y,x_1,y_1)\right|^2 dx_1dy_1, \quad (2)$$

where $u(t) = s_r(t) + n(t)$ is the observation equation to be processed in the optimal algorithm. Equation (3) consists of an additive mixture of the useful signal and internal receiver noise. Equations (1) and (2) also include the following components: $W_u\left[t,t_1,\sigma^0(x,y)\right]$ is the inverse correlation function, $\dot{s}_0(t,x,y)$ is a unit useful signal that would be received by the antenna from a single point on the surface with coordinates (x,y) and a unit reflection coefficient, $\sigma^0(x,y)$ is the effective scattering area of the surface or the ideal radar image of the surface, $\hat{\sigma}^0(x,y)$ is an estimate of the radar image of the surface, distorted by the uncertainty function $\left|\dot{\Psi}(x,y,x_1,y_1)\right|^2$ of the system.

The first equation represents the basic operations that must be performed on $u(t)$ to obtain an estimate of the radar image of the surface. The second equation describes the physics of the process of forming a radar image of the surface and indicates that the estimate $\hat{\sigma}^0(x,y)$ is a convolution of the real image with the uncertainty function of the system. The estimates in (1) and (2) are not identical, since the first equation contains an unaveraged residual of internal noise. To obtain equality between (1) and (2) in practice, raw radar images are additionally filtered using digital filters [10, 11]. The authors of this work have already developed a simulation model based on algorithm (2). In this study, the main focus is on modelling based on the mathematical operations in (1).

To specify the main operations in (1), it is necessary to define the unit useful signal $\dot{s}_0(t,x,y)$ model. For CW-LFM SAR we have

$$\dot{s}_0(t,x,y) = \dot{A}e^{j2\pi f_0 t}e^{-j2\pi f_0 2R_0(y)c^{-1}}\times$$
$$\times e^{-j2\pi f_0(Vt-x)^2 R_0^{-1}(y)c^{-1}}\times$$
$$\times\sum_{i=0}^{\infty}\Pi_P(t-iT_P-2R_0(y)c^{-1}-(Vt-x)^2R_0^{-1}(y)c^{-1})\times$$
$$\times\sum_{k=0}^{K}\Pi_s(t-iT_P-k\Delta t-2R_0(y)c^{-1}-(Vt-x)^2R_0^{-1}(y)c^{-1})\times$$
$$\times e^{j2\pi(\alpha k\Delta t)(t-iT_P-2R_0(y)c^{-1}-(Vt-x)^2R_0^{-1}(y)c^{-1})}, \quad (3)$$

where A is the constant amplitude of the probing signal, $e^{-j2\pi f_0 t}$ is the carrier oscillation at frequency f_0, $R_0(y)$ is the slant range, c is the propagation speed of electromagnetic waves, V is the speed of rectilinear motion of the carrier, $\Pi_P(t-iT_P)$ is the rectangular pulse determining the length of one period of the FM signal, T_P is the period of the sawtooth function of frequency change, i is the modulation period number, $\Pi_s(t-iT_P-k\Delta t)$ is the rectangular pulse determining the duration of a part of the FM signal within one period and having a constant frequency value, Δt is the time interval during which the signal frequency does not change, k is the pulse number of $\Pi_s(\cdot)$, $\alpha = \dfrac{(F_{\max}-f_0)}{T_p}$ is the slope of the sawtooth frequency variation function, $(F_{\max}-f_0)$ is the frequency deviation, $F_{\max}$ is the maximum frequency that the FM modulated signal can take.

Substituting (3) into (1) a structural diagram of an airborne radar for radar imaging using CW-LFM signals was developed. This diagram is presented in Fig. 1.

The radar operates as follows. A CW-LFM signal is generated in the probe signal generator, which is then converted into electromagnetic waves by antenna A1 for transmission toward the surface being investigated. Part of the signal is fed into the receiving channel via a directional coupler, creating a reference high-frequency coherent signal. Electromagnetic waves reflected from the surface are received by antenna A2 and converted into a received signal. The first optimal processing operation consists of quadrature detection of the received signals, or, in other words, multiplying the time-delayed emitted signal and its quadrature component by the received signal, which is performed in an IQ mixer. At the output of the IQ mixer, we will have direct and quadrature signals at an intermediate frequency.

The next optimal operation is to determine the discrete Fourier transform by range in the DFT block. However, there is no need to determine all possible ranges from 0 to infinity; it is better to limit ourselves to

the actual conditions of the experiment and determine the minimum and maximum ranges. The defined range of distances is proportional to the range of difference frequencies, so to simplify the requirements for the analog-to-digital converter (ADC block), a bandpass filter is installed after the multiplier. After quadrature detection, the signals sequentially pass through a Bandpass filter, an ADC, and a DFT calculation device. At the DFT output, for each of the components, we have a two-dimensional process that varies in time and range coordinate.

Further processing is performed in time and implements the synthesis of the antenna aperture in azimuth. To do this, the entire data array is divided into range rows, and in the Discrete convolution block, each row is convolved with a reference low-frequency function, which is generated in the Reference low-frequency function bank block and decorrelated in the Inverse filter. The square of the modulus is determined based on the convolution result. After convolving each row of the array at the output of the Discrete convolution block and determining the square of the modulus from the resulting array, we obtain a primary radar image, which requires averaging over the ensemble of realisations. Since it is impossible to fly over the same area multiple times in most practical tasks, it is necessary to implement an analogue of averaging over the ensemble of realisations – digital filtering with certain windows. There are many filtering methods, and their analysis is given in [12-15]. The filtering result is fed to the Storage or display block.

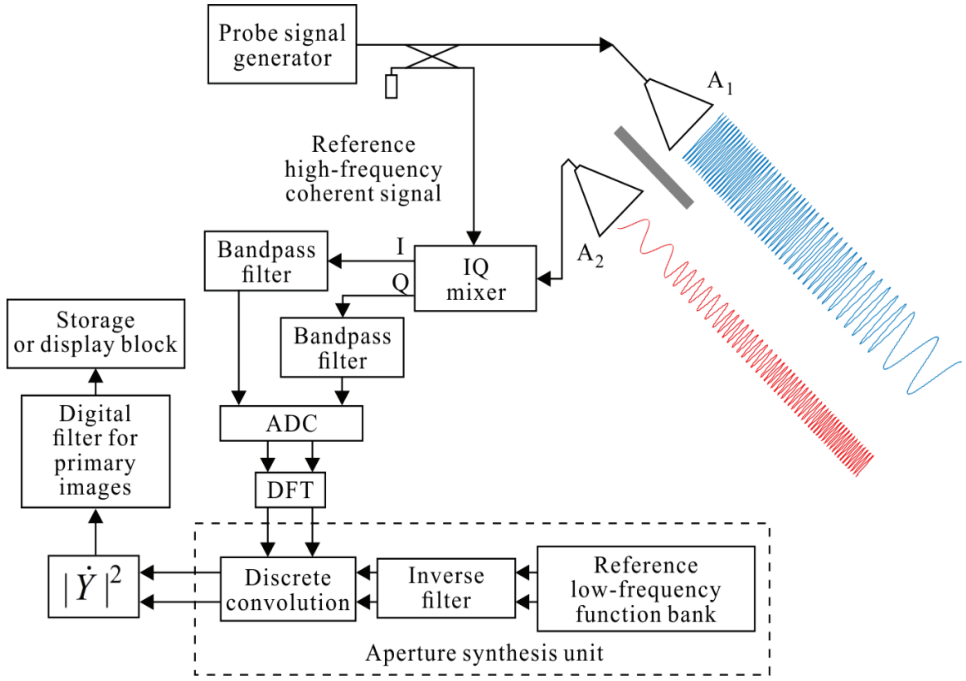

Fig. 1 - Block diagram of an airborne radar system for surface imaging using CW-LFM signals

Simulation model for radar imaging algorithms approbation

A simulation model for the developed radar block diagram is shown in Fig. 2. All experiments were implemented in MATLAB R2022a. Computations were CPU-only (16 GB RAM, 3200 MT/s). Each cycle processed ~781 MB of data and took 40 minutes of wall-clock time. The model contains almost all the main operations of optimal signal processing from the proposed radar block diagram. The only addition is the operation of forming a test ideal complex surface scattering coefficient $\dot{F}(x,y)$, which is theoretically white Gaussian noise with zero mathematical expectation and the following correlation function

$$R_{\dot{F}}(x_1,x_2,y_1,y_2)=\left\langle \dot{F}(x_1,y_1)\dot{F}(x_2,y_2)\right\rangle = \\ =\sigma^0(x_1,y_1)\delta(x_1-x_2)\delta(y_1-y_2), \quad (4)$$

where $\langle\cdot\rangle$ is the sign of statistical averaging over the ensemble of realisations (mathematical expectation). It is impossible to generate a realisation $\dot{F}(x,y)$ with an infinite spectrum on a computer, so the following discrete model was chosen

$$\dot{F}(x_i,y_i)=\sqrt{0{,}5\sigma^0(x_i,y_i)}\dot{\xi}(x_i,y_i)= \\ =\sqrt{0{,}5\sigma^0(x_i,y_i)}\left[\mathrm{Re}\left\{\dot{\xi}(x_i,y_i)\right\}+j\,\mathrm{Im}\left\{\dot{\xi}(x_i,y_i)\right\}\right], \quad (5)$$

where $\mathrm{Re}\dot{\xi}(\vec{r})$ and $\mathrm{Im}\dot{\xi}(\vec{r})$ are spatial delta-correlated processes with unit spectral power density, $\sigma^0(x_i,y_i)$ is a discrete ideal radar image of the surface.

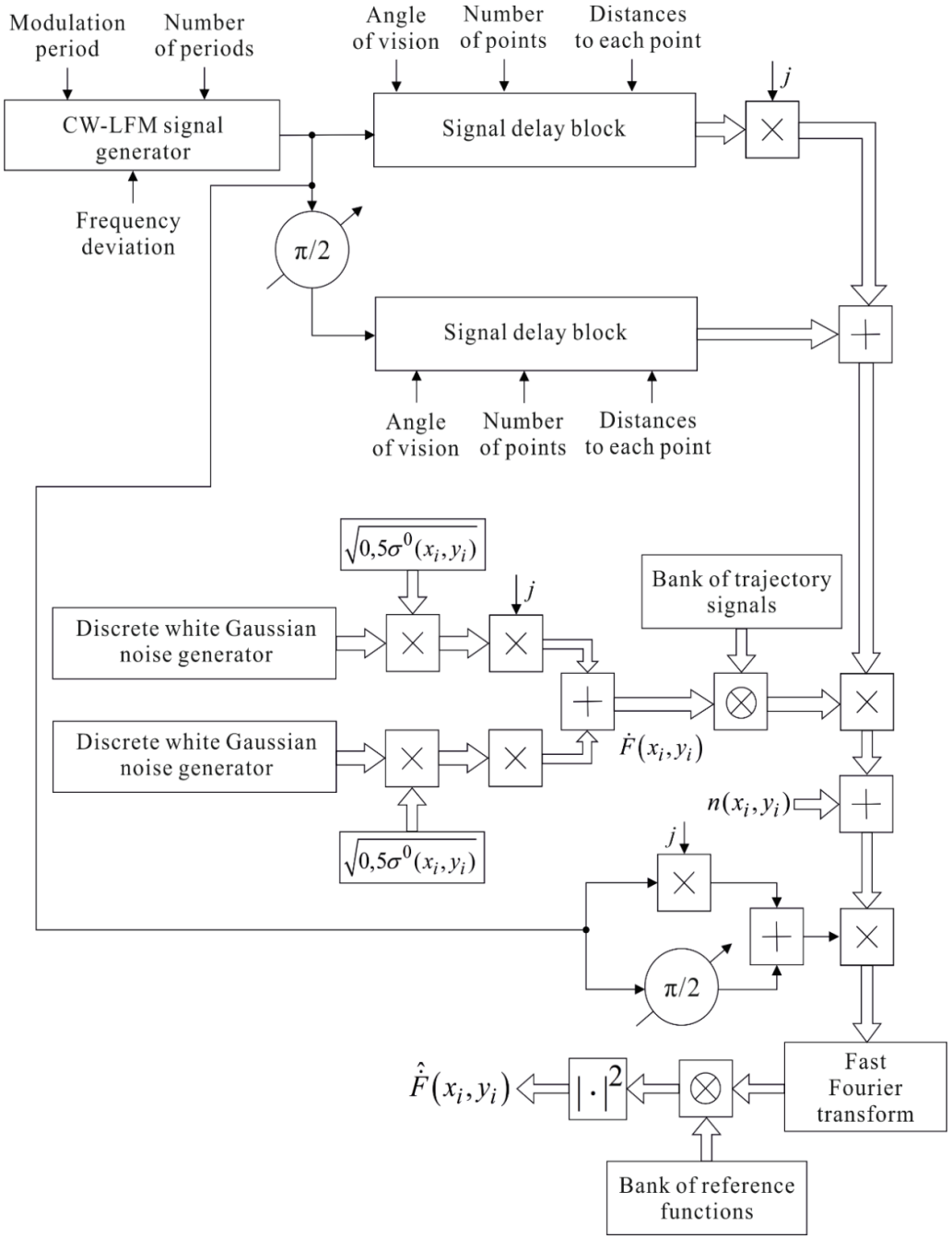

Fig. 2 – Simulation model of airborne radar surface imaging using CW-LFM signals

Analysis of simulation modelling results

In this paper, the SAR raw signal processing is performed in the two-dimensional frequency domain using the Omega-k algorithm, which consists of general focusing and differential focusing, and from this point onward this algorithm is considered as classical [16]. The test radar image and the results of its restoration by classical and synthesised methods are shown in Fig. 3.

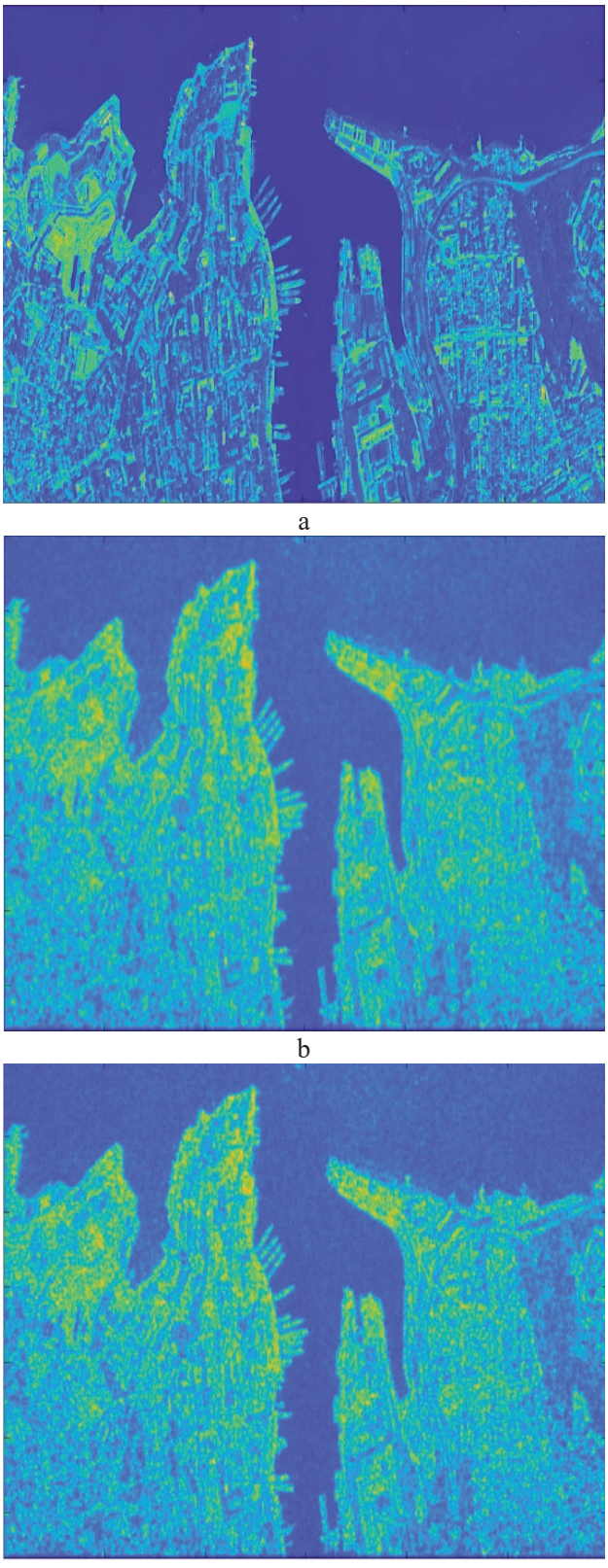

Fig. 3 - Radar images of the surface: a - ideal test image, b - obtained by the classical method, c - obtained with the decorrelation operation

According to the results of qualitative analysis of the obtained images, it follows that the proposed new optimal operation of decorrelation of the reference signal does not distort the result, and the proposed algorithm is workable. To assess the quantitative indicators, metrics of image quality comparison with the reference were used. Let us consider these metrics in more detail.

The Average Difference (AD) metric calculates the average difference between the pixels of the reference and distorted image. This is a simple metric that measures the average deviation. The AD metric is a well-known basic metric in image processing, often mentioned in the literature on image quality assessment as a simple statistical characteristic [17].

The Feature Similarity Extended (FSE) metric uses the division of the image into regions (edges, textures, flat) and calculates a similarity index based on SSIM (Structural Similarity Index) for each region with subsequent weighting. This is an extended metric that takes into account the features of the image content. It is not a standard metric from widely known publications, but similar approaches to image content analysis appear in works [18]. As a region-wise SSIM aggregate, FSE is sensitive to local degradations (defocus, sidelobes, speckle-induced contrast), so it can deviate from 1 even with high correlation.

Structural Similarity Index (SSIM) metric evaluates image quality based on brightness, contrast, and structural information. It uses a local window (Gaussian by default) and returns the mean value and a similarity map [19]. SSIM is local and drops with slight PSF, being window/scale-dependent, it is more sensitive than energy-based measures.

Normalised Cross-Correlation (NCC) measures the similarity between a reference and a distorted image by normalising the product of their pixel values by the sum of squares of the values of the reference image. A value close to 1 indicates high similarity. A classic metric in image processing [17], often used for image comparisons as a simple correlation measure. NCC is scale-invariant and tolerant to mild smoothing, so it often stays close 1.

Noise Quality Measure (NQM) metric is a nonlinear weighted metric for estimating additive noise. It uses a log-cosine bank filter to decompose the image into frequency bands, takes into account contrast thresholds and suprathreshold perceptual effects. The result is expressed in decibels [20].

Peak Signal-to-Noise Ratio (PSNR) is a metric that calculates the ratio of the maximum possible signal power to the noise power, expressed in decibels. It is based on the mean square error (MSE) between the reference and distorted images. In the case of zero error (MSE = 0), a conditional value of 99 dB is returned. This is a classic metric

widely used in image and signal processing. It is mentioned in the literature, for example, in [19].

The mean square error (MSE) between the reference and distorted images is one of the most common quality assessment metrics. A classic metric, described in [17].

The Structural Content (SC) metric calculates the ratio of the sum of squares of the pixel values of the reference image to the sum of squares of the values of the distorted image. It is used to estimate structural similarity based on signal energy values near 1 indicate energy match, not preservation quality of structure. It is mentioned as a simple metric in early works on image quality assessment [21].

The SVD-Based Image Quality Measure (SVD IQA) image quality metric is based on the singular decomposition (SVD). It calculates a graphical (spatial) and numerical quality assessment by comparing the singular values of the blocks of the reference and distorted images. It is described in detail in [22].

Visual information fit (VIF) metric evaluates image quality by comparing a reference and a distorted image. It uses a steerable pyramid for subband decomposition and a noise model to estimate the stored information. It returns a value in the range [0, 1], where 1 is perfect quality. VIF penalises high-frequency information loss, so it is sensitive to defocus, sidelobe leakage, and speckle decorrelation. The metric is given in [23].

The result of calculating these metrics for the images obtained in Fig. 3 is shown in Table 1.

Table 1. Quantitative indicators of the quality of radio image formation

Name of the metric for comparing image quality with a standard	Perfect test radar image	Radar image obtained by the classical method	Radar image obtained using the decorrelation method
AD	0	16.0394	16.3491
FSE	1	0.3860	0.4673
SSIM	1	0.5638	0.6262
NCC	1	0.9887	0.9893
NQM	∞	13.6155	13.6268
PSNR	99	19.0089	19.2281
MSE	0	816.9412	776.7219
SC	1	0.9016	0.9015
SVD IQA	0	22.1278	22.4622
VIF	1	0.2476	0.2541

The small differences reported for the metrics – NCC 0.9887 *vs* 0.9893 $\left(\Delta \approx 6\times10^{-4}\right)$ and SC 0.9016 *vs* 0.9015 $\left(\Delta \approx 1\times10^{-4}\right)$ – fall within the expected numerical/estimation uncertainty of the processing (finite-precision FFT, interpolation, registration). They are not statistically or practically significant and do not establish an advantage of one method over the other for this dataset.

Based on the analysis of Table 1, the image formed with decorrelation outperforms the classical result across most metrics. These findings are preliminary and were obtained under a relatively high signal-to-noise ratio (SNR ≈ 20 dB). A rigorous quantification of azimuthal defocus and radiometric distortions, as well as geometric deformations induced by phase errors due to nonuniform platform motion, warrants further investigation.. The gain in quality is not measured in hundreds of percent and not many times greater, but this approach is fruitful and requires further development. Let us analyse the relative improvement in the quality of radar image restoration as a result of simulation modelling of the following uncertainty function

$$\dot{\Psi}(x,y,x_1,y_1)=\int_0^T \dot{s}_0(t_1,x,y)\,\dot{s}^*_{0W}(t_1,x_1,y_1)dt_1 \quad (6)$$

For this purpose, Fig. 4 shows the spectrum of the reference signal in azimuth $e^{-\frac{j2\pi f_0(Vt-x)^2}{R_0(y)c}}$ for one range and the spectrum of this signal after its decorrelation. From the given graphs, it follows that the optimal algorithm increases the frequency components in the received signals that were suppressed by the spectrum of the probing signal. The degree of extraction of the suppressed spectral components depends on the signal-to-noise ratio. For the given spectrum and the radar image in Fig. 4, the signal-to-noise ratio was 20 dB. The given processing was performed in the spectrum and after applying the inverse Fourier transform in Fig. 5 and Fig. 6 for comparison, the reference signals for synthesising radio images in azimuth for the classical and new methods are given. As can be seen from the obtained graphs, significant amplitude emissions appear at the beginning and end of the reference signal with decorrelation. The result of using such a reference signal is shown in Fig. 7.

The vertical brightness band in the restored radar image is associated precisely with artifacts in the reference signal. The appearance of such amplitude outliers is caused by the finite duration of the discrete real output signal. $e^{-\frac{j2\pi f_0(Vt-x)^2}{R_0(y)c}}$ and the finiteness of the spectrum of this signal. To eliminate the above-mentioned shortcomings of real processing, a weighting function was applied, which significantly reduced the amplitude of the reference signal at its beginning and end, as shown in Fig. 8. The result of using the modified reference signal

with decorrelation was already demonstrated in Fig. 3, c. In this figure, it follows that artifacts are now absent.

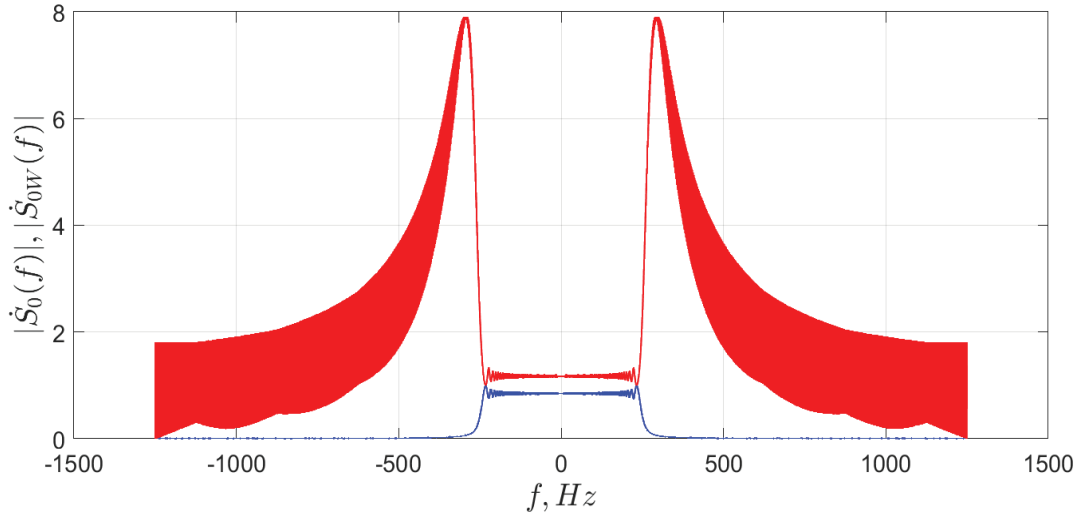

Fig. 4 - Amplitude spectra: blue line - reference signal for compression of radar measurements in azimuth with classical processing, red line - reference signal for compression of radar measurements in azimuth after inverse filtering

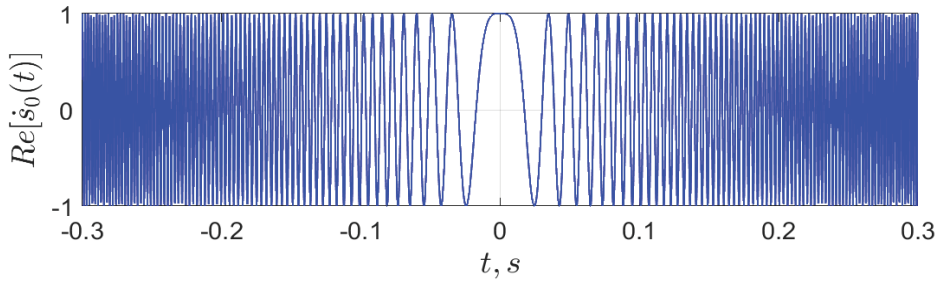

a

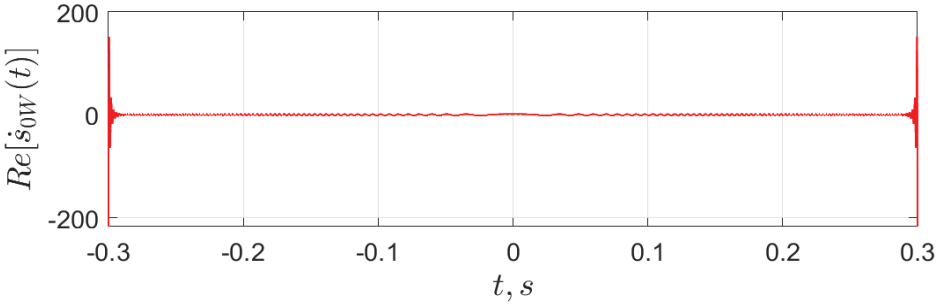

b

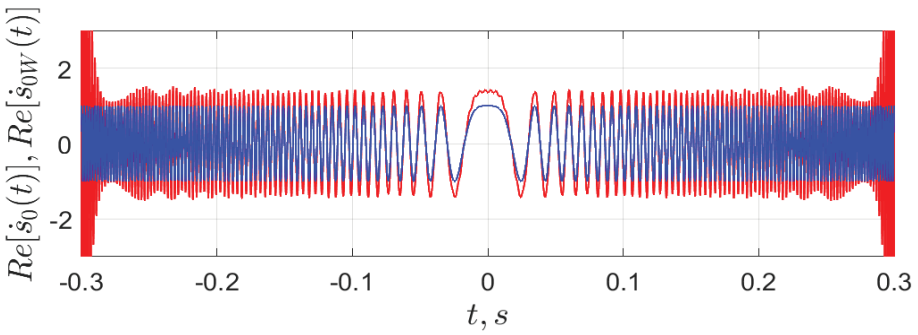

c

Fig. 5 - Direct reference signal for compression of radio measurements by azimuth coordinate: a - classical method, b - new synthesised method

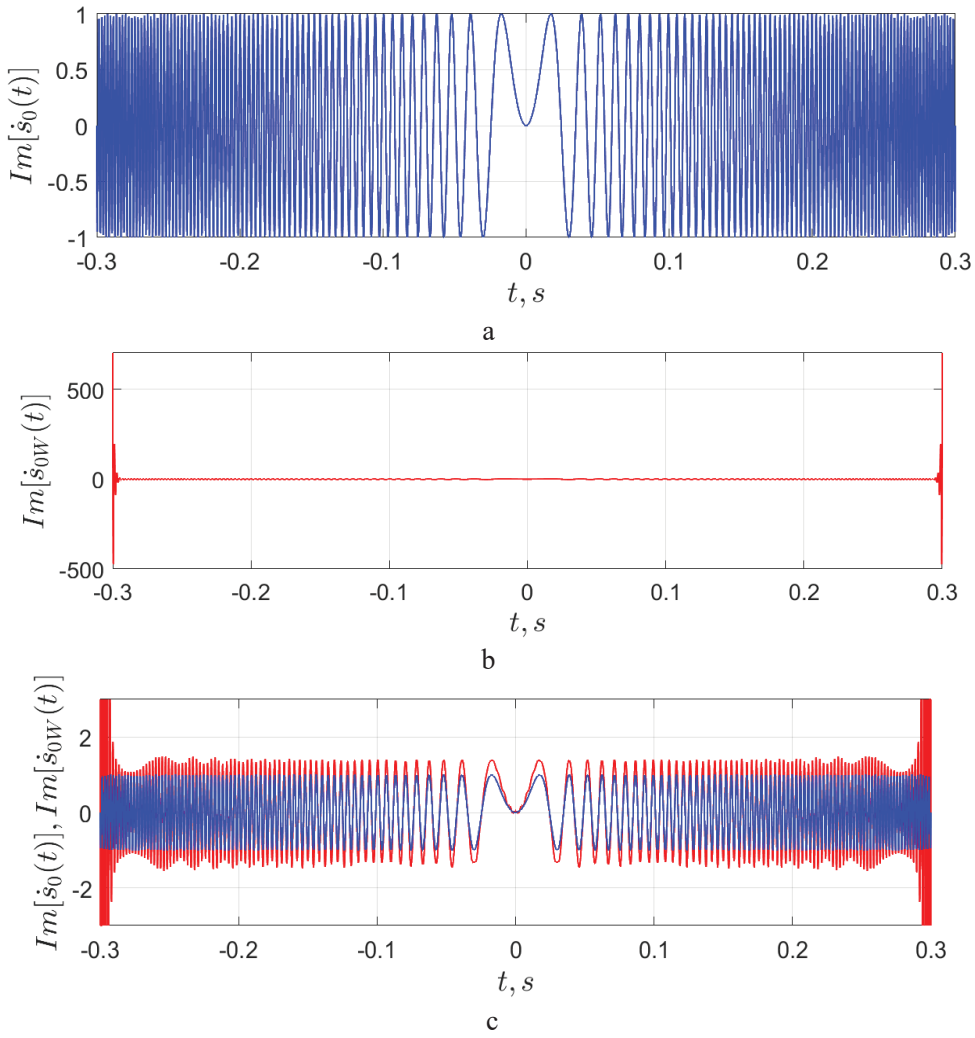

Fig. 6 - Quadrature reference signal for compression of radio measurements by azimuth coordinate: a - classical method, b - new synthesised method

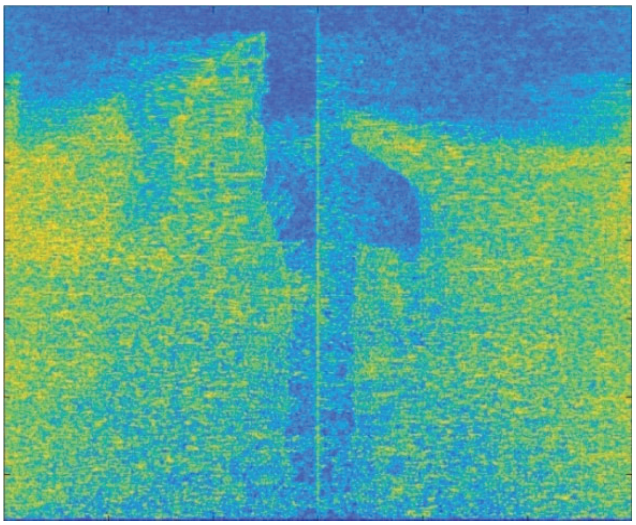

Fig. 7 - Example of a reconstructed radar image using a decorrelated reference signal with artifacts

Having determined all the features of the formation of the reference signal with decorrelation, Fig. 9 shows the decoherence function of the radio vision radar system in azimuth. The graphs display the result of calculating formula (6) in surface coordinates using the classical radio vision method and the method synthesised in this section using the decorrelation operation. Decorrelation was performed for a signal-to-noise ratio of 20 dB. It follows from the obtained graphs that the decoherence function is twice as narrow when using the modified method, but also has twice as high side lobes. To reduce the influence of side lobes, it is possible to use more optimal and effective weight windows for the reference signal after decorrelation. In general, the effect of using decorrelating filters in processing can be estimated at 18-20% quality improvement, according to the analysis of the metrics given in Table 1.

Let the measured spectrum be:

$$Y(f) = H(f)X(f) + N(f) \qquad (7)$$

where $X(f)$ is the scene spectrum, $H(f)$ is the system/processing transfer function (including the reference function before decorrelation), and $N(f)$ is additive noise. An unregularized inverse filter $G_{inv}(f)=\frac{1}{H(f)}$ produces:

$$\hat{X}(f)=G_{inv}(f)Y(f)=X(f)+\frac{N(f)}{H(f)} \quad (8)$$

Hence the output-noise PSD is scaled by $|1/H(f)|^2$ near spectral notches of $|H(f)|$ A regularized Wiener-type inverse

$$G_{reg}(f)=\frac{H^*(f)}{|H(f)|^2+\frac{S_N(f)}{S_X(f)}} \quad (9)$$

ties the amount of spectral recovery directly to the local SNR S_X/S_N at moderate-to-high SNR one has $G_{reg}(f)\approx\frac{1}{H(f)}$, [16] so suppressed components are effectively recovered and the useful spectral support is broadened, whereas at low SNR the denominator in $|G_{reg}(f)|$, preventing noise amplification. For implementation, an equivalent and convenient form is

$$G_{reg}(f)=\frac{H^*(f)}{|H(f)|^2+\lambda} \quad (10)$$

estimated from pre-image noise or homogeneous focused patches, making decorrelation SNR-adaptive. As a whitening step, it reduces speckle and increases ENL at higher SNR [12, 15]. As in Fig. 9, main-lobe narrowing raises sidelobes; suppress them with post-decorrelation weighting (e.g., Kaiser/Hamming) tuned to the target PSLR/ISLR.

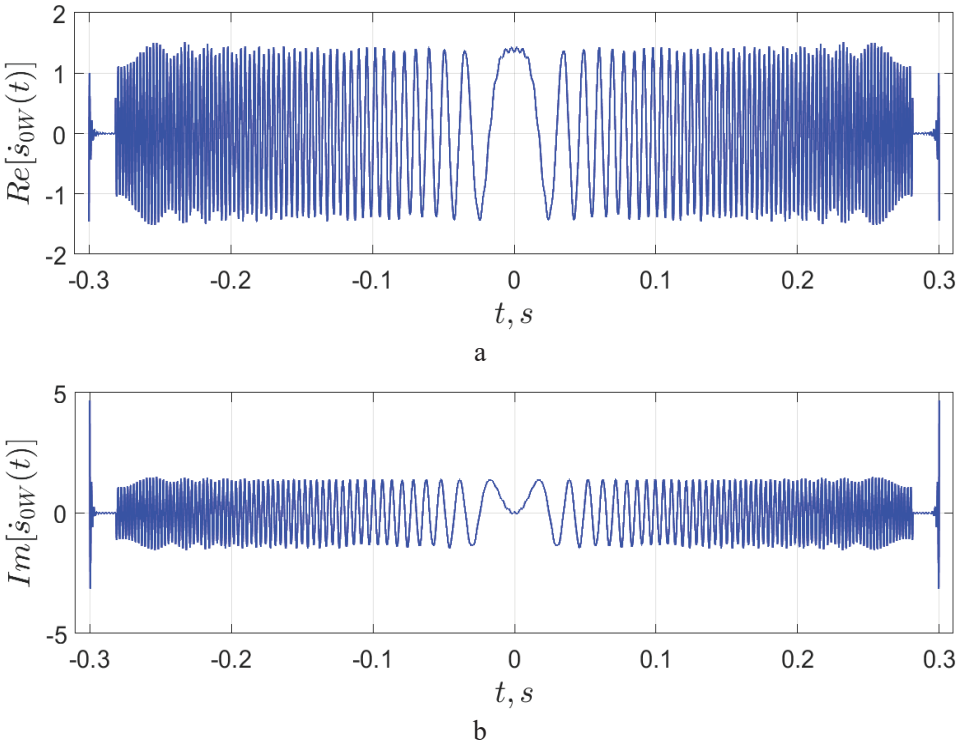

Fig. 8 - Reference signals after their correction: a - direct, b – quadrature

For the given simulation the test image was formed by converting a full-colour high-resolution optical satellite image into a grayscale image. This approach is visual, but not entirely correct, because the optical image used already contained its own sensor noise, which can distort the analysis result. To assess the improvement of the quality of the proposed signal processing, a simulation modelling of the process of forming radio images with an artificially synthesized test image in vector image processing packages was carried out. The test image and its restoration result by classical and synthesised methods are shown in Fig. 10 and Fig. 11. Quality analysis according to the metrics already considered is given in Table. 2.

The results obtained in Table 2 confirm the fact of increasing the accuracy of radio image reconstruction when using the decorrelation operation. It should be noted that for an artificially created image, all metrics showed an increase in the quality of radar image formation when using decorrelation. Another physical justification for the increase in accuracy is the fact that the decorrelation filter at high signal-to-noise ratios brings the received signal closer to white noise. In this case, the size of the speckles in the primary radar image decreases in width, and the number of these speckles within the secondary processing filter increases. As a result of the specified increase in the number of speckles, the averaging result becomes more effective, which is equivalent to increasing the resolution of the radar image. Confirmation of the presence of new information in the primary radar image is the modulus of the difference between the primary radar image obtained by the classical method and the radar image formed with the decorrelated reference signal, shown in Fig. 12.

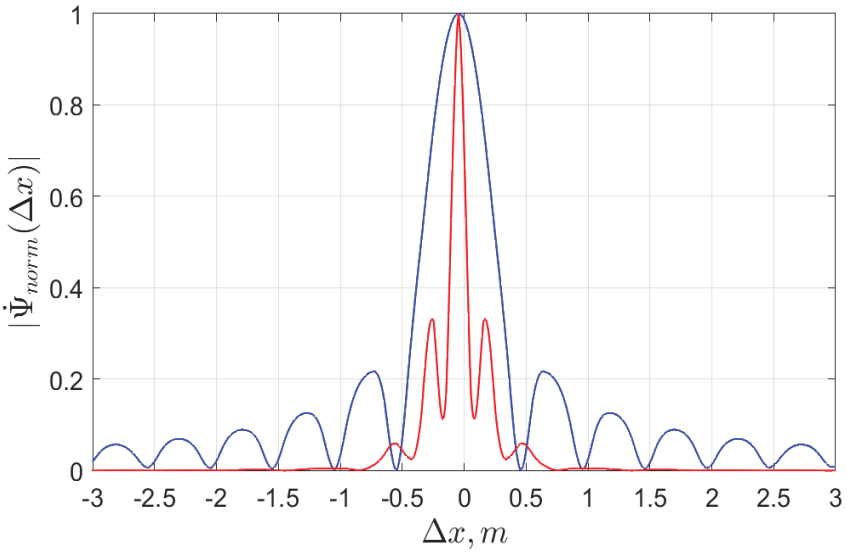

Fig. 9 - SAR uncertainty function in azimuth coordinate: blue line - classical processing method, red line - processing with decorrelation of the reference signal

Table 2. Assessment of the quality of radio image restoration using an artificially synthesised test image

Name of the metric for comparing image quality with a standard	Perfect test radar image	Radar image obtained by the classical method	Radar image obtained using the decorrelation method
AD	0	7.2512	6.6965
FSE	1	0.4608	0.5205
SSIM	1	0.6859	0.7543
NCC	1	0.9962	0.9967
NQM	∞	13.8524	14.0671
PSNR	99	23.4973	24.1040
MSE	0	290.6391	252.7452
SC	1	0.9469	0.9517
SVD IQA	0	21.3659	20.1114
VIF	1	0.3211	0.3260

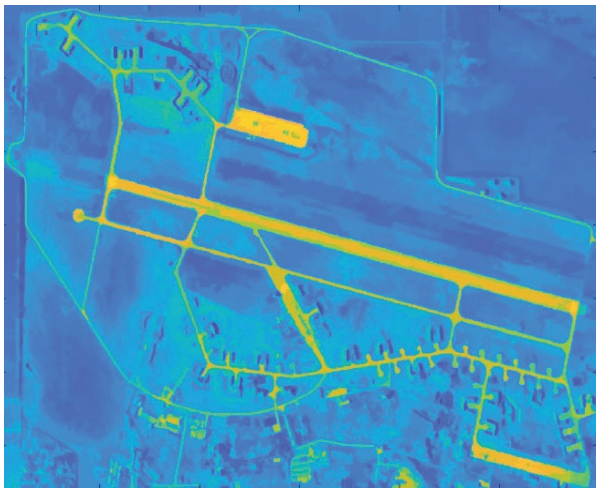

Fig. 10 – An ideal artificially created test radar image of the surface

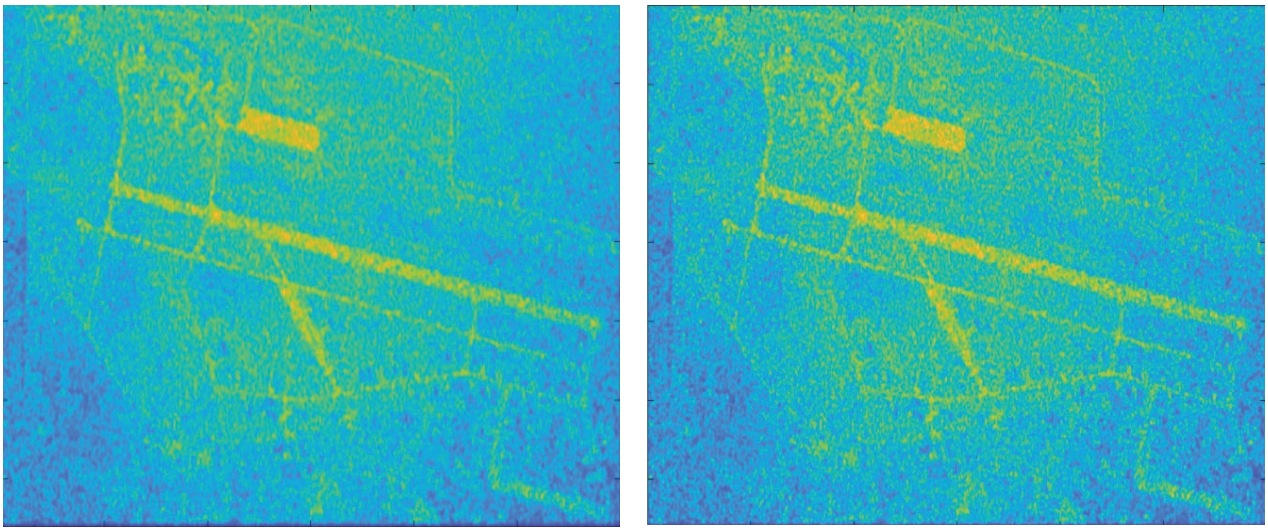

a b

Fig. 11 - Radar images of the surface: a - obtained by the classical method, b - obtained with the decorrelation operation

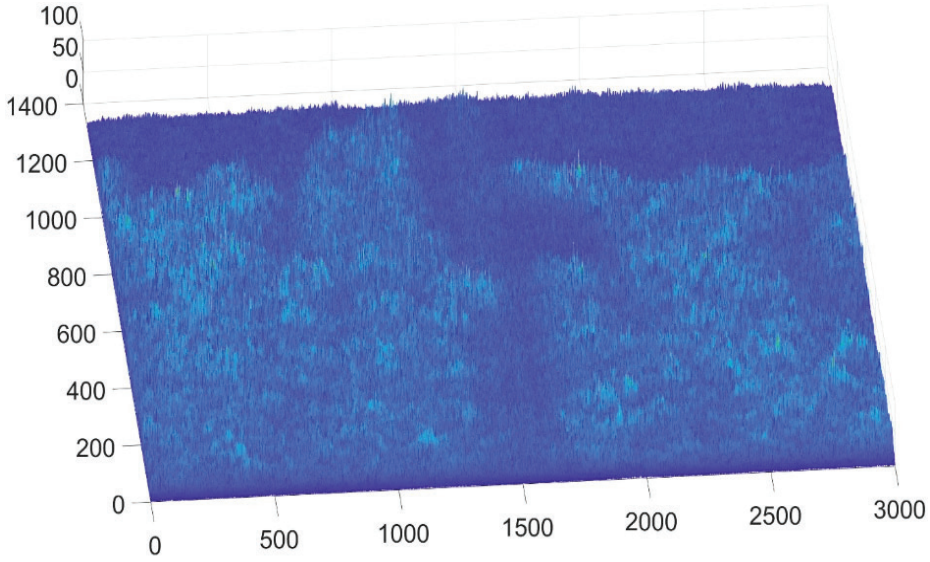

Fig. 12 - Difference modulus of primary radar images formed by the classical and synthesised new method

References

1. Wang, Yaping, Tianjiao Zeng, Xu Zhan, Xiangdong Ma, Mou Wang, Jun Shi, Shunjun Wei, and Xiaoling Zhang. 2024. "High-Quality Short-Range Radar Imaging with Coprime Sampling" Remote Sensing 16, no. 24: 4657. Retrieved from: https://doi.org/10.3390/rs16244657

2. Golkar, A., Cataldo, G., & Osipova, K. (2021). Small satellite synthetic aperture radar (SAR) design: A trade space exploration model. Acta Astronautica, 187, pp. 458–474. Retrieved from: https://doi.org/10.1016/j.actaastro.2021.07.009

3. Guan, Tianyue, Sheng Chang, Chunle Wang, and Xiaoxue Jia. 2025. "SAR Small Ship Detection Based on Enhanced YOLO Network" Remote Sensing 17, no. 5: 839. Retrieved from: https://doi.org/10.3390/rs17050839

4. Işıker, H., & Özdemir, C. (2020). Adaptation of stepped frequency continuous waveform to range-Doppler algorithm for SAR signal processing. Digital Signal Processing, 106, 102826. Retrieved from: https://doi.org/10.1016/j.dsp.2020.102826

5. Zhou, D., & Zhao, Z. (2024). Optimal algorithm for distributed scatterer InSAR phase estimation based on cross-correlation complex coherence matrix. International Journal of Applied Earth Observation and Geoinformation, 134, 104214. Retrieved from: https://doi.org/10.1016/j.jag.2024.104214
6. Volosyuk, Valeriy, and Semen Zhyla. 2022. "Statistical Theory of Optimal Stochastic Signals Processing in Multichannel Aerospace Imaging Radar Systems" Computation 10, no. 12: 224. Retrieved from: https://doi.org/10.3390/computation10120224
7. Volosyuk, V., Pavlikov, V., Zhyla, S., Popov, A., Ruzhentsev, N., Tserne, E., Kolesnikov, D., Vlasenko, D., Kosharskyi, V., Inkarbaieva, O., Cherepnin, G., & Kovalchuk, D. (2024). THEORY OF CLASSICAL AND MODIFIED SPACEBORNE SYNTHETIC APERTURE RADAR IMAGING. Advances in Space Research. Retrieved from: https://doi.org/10.1016/j.asr.2024.09.033
8. Cruz, Helena, Mário Véstias, José Monteiro, Horácio Neto, and Rui Policarpo Duarte. 2022. "A Review of Synthetic-Aperture Radar Image Formation Algorithms and Implementations: A Computational Perspective" Remote Sensing 14, no. 5: 1258. Retrieved from: https://doi.org/10.3390/rs14051258
9. David Stewart, Rod Cook, Ian McConnell, and Christopher John Oliver "Optimal processing techniques for SAR", Proc. SPIE 3500, Image and Signal Processing for Remote Sensing IV, (4 December 1998); Retrieved from: https://doi.org/10.1117/12.331883
10. D. Kolesnikov, S. Zhyla, V. Pavlikov and O. Mazurenko, "Imaging Simulation for Radar with Static Aperture Synthesis Method," 2023 IEEE International Conference on Information and Telecommunication Technologies and Radio Electronics (UkrMiCo), Kyiv, Ukraine, 2023, pp. 192-197. Retrieved from: doi: 10.1109/UkrMiCo61577.2023.10380361.
11. V. Volosyuk, S. Zhyla, D. Vlasenko, O. Inkarbaieva, D. Kolesnikov and G. Cherepnin, "Concepts of Primary and Secondary Coherent Images in Radar and Optical Systems," 2022 IEEE 3rd International Conference on System Analysis & Intelligent Computing (SAIC), Kyiv, Ukraine, 2022, pp. 1-6. Retrieved from: doi: 10.1109/SAIC57818.2022.9923005.
12. Pan, Ting, Dong Peng, Wen Yang, and Heng-Chao Li. 2019. "A Filter for SAR Image Despeckling Using Pre-Trained Convolutional Neural Network Model" Remote Sensing 11, no. 20: 2379. Retrieved from: https://doi.org/10.3390/rs11202379
13. Li, Y., Wang, S., Zhao, Q., & Wang, G. (2020). A new SAR image filter for preserving speckle statistical distribution. Signal Processing, 176, 107706. Retrieved from: https://doi.org/10.1016/j.sigpro.2020.107706
14. Guo, Fengcheng, Chuang Sun, Ning Sun, Xiaoxiao Ma, and Wensong Liu. 2023. "Integrated Quantitative Evaluation Method of SAR Filters" Remote Sensing 15, no. 5: 1409. Retrieved from: https://doi.org/10.3390/rs15051409
15. Rubel, Oleksii, Vladimir Lukin, Andrii Rubel, and Karen Egiazarian. 2021. "Selection of Lee Filter Window Size Based on Despeckling Efficiency Prediction for Sentinel SAR Images" Remote Sensing 13, no. 10: 1887. Retrieved from: https://doi.org/10.3390/rs13101887
16. Jancco-Chara, J., Palomino-Quispe, F., Coaquira-Castillo, R.J., Herrera-Levano, J.C., Florez, R. 2024. "Doppler Factor in the Omega-k Algorithm for Pulsed and Continuous Wave Synthetic Aperture Radar Raw Data Processing" Applied Sciences 14: 320. Retrieved from: https://doi.org/10.3390/app14010320
17. C. Gonzalez E. Richard "Digital Image Processing," Pearson education, 2018, pp. 993.
18. Lei Zhou, Chuanlin Liu, Amit Yadav, Sami Azam Asif Karim, "Image Quality Assessment Based on Edge and Texture Information," Machine Vision and Applications, 2024. Retrieved from: doi.org/10.1007/s00138-024-01522-6
19. Zhou Wang, A.C. Bovik, H.R. Sheikh, E.P. Simoncelli, Image Quality Assessment: From Error Visibility to Structural Similarity," IEEE Transactions on Image Processing, Vol. 13, No. 4. 2004, pp. 600 – 612. Retrieved from: doi: 10.1109/TIP.2003.819861
20. Damera-Venkata, N., Kite, T. D., Geisler, W. S., Evans, B. L., Bovik, A. C. (2000). "Image Quality Assessment Based on a Degradation Model," IEEE Transactions on Image Processing, Vol. 9, No. 4., 2000, pp. 636 – 650. Retrieved from: doi: 10.1109/83.841940.
21. A. M. Eskicioglu, P. S. Fisher, "Image Quality Measures and Their Performance," IEEE Transactions on Communications. 1995, pp. 2959-2965. Retrieved from: dx.doi.org/10.1109/26.477498
22. A. Shnayderman, A. Gusev, A. M. Eskicioglu, "An SVD-Based Grayscale Image Quality Measure for Local and Global Assessment," IEEE Transactions on Image Processing, Vol. 15, No. 2., 2006, pp. 422 – 429. Retrieved from: doi.org/10.1109/TIP.2005.86060
23. Minghua Zhao, Yong Fan, Yonghong Zhang, Zongrui He, "The W-Band High Order Avalanche Diode Frequency Multiplie," Int J Infrared Milli Waves, 2007, pp. 663–669. Retrieved from: doi 10.1007/s10762-007-9238-4

Павліков В.В., Жила С.С., Ковальчук Д.І., Колесніков Д.В., Сидоров Я.Д.

Імітаційна модель методу формування зображень в радарах з безперервними лінійно-частотно модульованими сигналами

Національний аерокосмічний університет імені М. Є. Жуковського Харківський авіаційний інститут, Харків, Україна

Проблематика. Сучасні системи радарів із синтезованою апертурою (РСА) мають вирішальне значення для спостереження за Землею, особливо в умовах, коли традиційні оптичні системи не справляються зі своїм завданням, наприклад, при поганій видимості або несприятливих погодних умовах. Безперервні сигнали з лінійною частотною модуляцією (Б-ЛЧМ сигнали) є перспективними завдяки своїй енергоефективності та спрощеній апаратній реалізації, але вони ставлять значні завдання в області обробки сигналів, включаючи збереження фазової когерентності та видалення спектральних артефактів.

Мета досліджень. Дослідження має на меті розробку та моделювання структурної моделі компактної системи РСА на основі Б-ЛЧМ сигналів, з акцентом на поліпшенні якості зображення за допомогою вдосконалених алгоритмів обробки сигналів, зокрема використання методів декореляції для опорних сигналів.

Методика реалізації. Дослідження включає математичну формулювання процесів радіолокаційного зображення, розробку імітаційної моделі на основі запропонованої структурної схеми та реалізацію операцій обробки сигналів, таких як квадратурне виявлення, дискретні перетворення Фур'є та цифрове фільтрування. Впроваджено новий метод декореляції опорних сигналів, який оцінено порівняно з класичними підходами з використанням різних показників якості зображення.

Результати досліджень. Результати моделювання показують, що запропонована техніка декореляції покращує показники якості зображення, включаючи SSIM, PSNR і NCC. Цей метод допомагає зменшити розмір спекл і підвищити роздільну здатність зображення. Артефакти, спричинені обмеженнями спектра, були ефективно придушені за допомогою функцій зважування. Кількісні оцінки з використанням як реальних, так і штучно створених радіолокаційних зображень підтвердили перевагу запропонованого методу над класичними техніками.

Висновки. Розроблена модель симуляції та вдосконалення обробки сигналів демонструють доцільність та ефективність використання систем Б-ЛЧМ РСА з покращеною декореляцією для отримання радіолокаційних зображень з високою роздільною здатністю. Отримані результати можуть бути використані для подальших досліджень та практичного застосування в компактних повітряних та безпілотних платформах для цивільних та оборонних цілей.

Ключові слова: *радар із синтезованою апертурою; Б-ЛЧМ сигнали; декореляція; імітаційна модель; показники якості зображення.*

Received by the Editorial Office
July 8, 2025

Accepted for publication
September 15, 2025